

River Channel Lateral Mobility: Metrics, Time Scales, and Controls

Andrew D. Wickert¹ John M. Martin² Michal Tal³ Wonsuck Kim⁴ Ben Sheets⁵
Chris Paola⁶

Abstract. Alluvial river channels are intrinsically mobile. We mapped channel planform extent in a series of experiments to measure instantaneous rates of channel motion, loss of planform overlap with the original positions of the channels, and reworking of the fluvial surface over which the channels moved. These experiments comprise two aggrading deltas, one subsiding delta that underwent cyclical base level changes, and one braided channel system that was seeded with vegetation. We find that the amounts of channel planform overlap and remaining unworked fluvial surface area both decay exponentially with time, and that these metrics and the instantaneously-measured rates of channel motion scale predictably with one another in spite of the different time scales of the processes they record. Rates of channel planform change increase with increasing sediment flux and bed and planform irregularity, and decrease with the establishment of riparian vegetation. Aggradation does not noticeably affect channel mobility, but induces avulsions that allow the channels to more rapidly rework the fluvial surface. Additional findings include that: (1) sediment flux in the braided experiment equals its rate of bar migration, (2) channel widths are normally distributed with time, and (3) we can use our channel mobility metrics to connect surface processes with the resultant fluvial stratigraphy.

1. Introduction

Alluvial river channels in non-incisional settings are highly mobile systems that interact dynamically with their beds, banks, and the fluvial surfaces such as braid plains, valleys, and alluvial fans, through which they flow. Their morphologic evolution is affected by sediment discharge, base level changes, riparian vegetation, and internally-generated bed and planform irregularities such as barforms and sinuosity. We present novel analyses of a series of physical experiments to understand how these basic controls on morphodynamic change control overall rates of channel mobility across multiple time scales of measurement.

We measure channel mobility over three time scales characteristic to fluvial systems. In the short term, we measure channel mobility as a continuous change in channel planform with time, which equates to a combination of lateral migration rate and avulsion magnitude times frequency. Over longer time scales, rivers gradually lose overlap with

and “forget” the shape their previous planforms. Over even longer time scales, rivers move across and rework the sediments of their fluvial surfaces.

We apply metrics for these three time scales of channel planform change to a set of analog material experiments [Kim et al., 2006a, b; Martin, 2007; Sheets et al., 2007; Tal and Paola, 2007, 2010]. Although simplifications in the experimental conditions limit our ability to explore the full range of channel planforms and rates of landscape change in natural systems, these experiments offer the advantage of complete, high-resolution data sets under controlled conditions, making them an attractive platform from which to develop this method. These systems were forced with different sediment discharges, base level changes, vegetation, and/or flow conditions. These differing inputs allow us to pick apart how external forcings control channel mobility, and analyses across the whole range of experiments show relationships among our measurements at different time scales.

2. Descriptions of Experimental Systems

We examined river channel planform change in a series of experimental fluvial systems generated at the Saint Anthony Falls Laboratory at the University of Minnesota (Table 1). We observed three experimental alluvial fan deltas (depositional systems) [Kim et al., 2006a, b; Martin, 2007; Sheets et al., 2007] and one braided river (transport system) to which riparian vegetation was added [Tal and Paola, 2007, 2010]. We observed these experiments during windows in which all of the inputs to each channel system remained approximately constant, and did not include any of the early time steps in which the channel had not yet developed a self-formed fluvial network. These experimental systems were predominantly braided owing to the relative ease of reproducing braiding versus meandering in noncohesive sediments in the laboratory [e.g., Howard, 2009; Tal and Paola, 2010]. In this section we introduce the river systems studied and their basic characteristics (Table 2).

Three of the four experiments in our study are deltaic systems. DB03-1 [Sheets et al., 2007] and DB03-2 [Martin,

¹Department of Geological Sciences and Institute of Arctic and Alpine Research, University of Colorado at Boulder, Boulder, Colorado, USA

²ExxonMobil Upstream Research Company, Houston, Texas, USA

³Aix-Marseille Université, CEREGE UMR 7330, Aix-en-Provence, France.

⁴Institute for Geophysics and Department of Geological Sciences, Jackson School of Geosciences, University of Texas, Austin, Texas, USA

⁵Barr Engineering Company, Minneapolis, Minnesota, USA

⁶Department of Earth Sciences, St. Anthony Falls Laboratory, and the National Center for Earth-surface Dynamics, University of Minnesota, Minneapolis, Minnesota, USA

2007] are alluvial fan delta experiments. Sediment discharge in DB03-2 was much lower than that in DB03-1; this resulted in DB03-2 having subcritical flow, a lower fan surface slope, and a much lower aggradation rate. Both of these deltas first prograded to a defined radius (2.5 m for DB03-1 and 2.8 m for DB03-2), after which base level (the water level in the basin) was raised at a rate that produced a purely aggradational delta of uniform size (i.e. depositional equilibrium). We sampled only the time period over which these deltas were in depositional equilibrium. XES02 [Kim et al., 2006a, b] is a subsiding alluvial fan delta that underwent cyclical changes in base level. We sampled this experiment at five different intervals to obtain a picture of the effects of base level changes on rates of channel planform change and reworking of the fan surface: the stillstand (XES02-SS), the slow cycle of base level rise and fall (XES02-SR, XES02-SF), and the rapid cycle of base level rise and fall (XES02-RR, XES02-RF). The final experiment that we analyzed is part of a set of experiments designed to study the interactions between braiding and riparian vegetation (referred to here as BV) [Tal and Paola, 2007, 2010]. The first stage of this experiment (BV-1) was characterized by steady state braiding in noncohesive sand under uniform discharge. The second stage (BV-2) consisted of repeated cycles of a 1-hour high flow and a 6-day low flow. Alfalfa seeds (*Medicago sativa*) were dispersed uniformly over the bed immediately after the end of each high flow. Plants colonized freshly deposited bars and areas of braidplain that were not inundated during low flow [Tal and Paola, 2007, 2010]. Cycling high and low discharge in conjunction with plant seeding led to a change in channel planform from braided to single-thread and the formation of a vegetated floodplain.

3. Data from Images of Experiments

We separated the fluvial surface into binary maps of regions that were occupied by the river system (“wet”, 1) and those that were unoccupied (“dry”, 0). We measured planform change by observing how these “wet” and “dry” areas changed. The major advantage of this method is that it does not require a spatially coherent channel, and can therefore work in both multi- and single-thread systems. This is essential for analyzing our largely braided experiments. Our methods are improved versions of those used by Wickert [2007], and are written in Matlab and Python.

3.1. Defining Fluvial Surface and River Channels

We defined the fluvial surface (F) by removing regions that a river channel could not occupy (Figure 2). $F = 1$ across the fluvial surface, and $F = 0$ in regions that were excluded from our analysis. For all of the experimental deltas, we exclude all areas that are inundated by the ocean (XES02: Kim et al. [2006a, b]; DB03-1: Sheets et al. [2007] DB03-2: Martin [2007]). In XES02 [Kim et al., 2006a, b]], we also exclude abandoned terraces produced during the cycles of rapid base level change. These terrace surfaces were dyed for identification, and after the river channel incised into them, it occupied a limited and consistent valley over the duration of our measurements. For the braided and vegetated river systems (BV-1 and BV-2, respectively: Tal and Paola [2007, 2010]), we used the entire 10 meter study reach, which excludes a combined 6 meters at the upstream and downstream ends of the flume in order to avoid the effects of these boundary conditions.

We separated the fluvial surface, $F = 1$, into binary matrices referred to as “channel maps”. These matrices, denoted K , consist of channel (“wet”, 1) and unoccupied fluvial surface (“dry”, 0). This “wet” vs. “dry” analysis has been performed extensively on fluvial system experiments [Cazanaci et al., 2002; Tal and Paola, 2007; Wickert, 2007;

Martin, 2007; Martin et al., 2009; Kim et al., 2010; Tal and Paola, 2010]. In each experiment, colored dye was injected into the water (Figures 1 and 2), making it straightforward to use a set range of color values to separate the channel from dry sediment and/or vegetation. We processed the images to increase the contrast in color parameters (red, green, blue, hue, saturation, brightness) between the channel and the rest of the image, and then used a threshold to generate the binary channel maps. We applied a smoothing filter to remove small-scale (1–2-pixel radius) noise due to small changes in lighting and dye intensity that otherwise would cause an inaccurately large difference to be reported between channel systems at adjacent time steps. While this filter did not solve all of the issues with noise in the image processing, it provided an improvement over earlier methods [e.g., Wickert, 2007; Martin et al., 2009].

3.2. Determining Channel Planform Change

We used the channel maps (Section 3.1) to measure instantaneous rates of channel planform change, loss of channel system overlap with previous channel patterns, and reworking of the fluvial surface as the channels sweep across it. These measures are summarized schematically in Figure 3.

3.2.1. Channel overlap

We measured the loss of planform overlap by comparing river channel patterns at two different times and varying the amount of time between these two observations. This method is a bulk variant of the method Sapozhnikov and Foufoula-Georgiou [1997] used to measure the spatial structure of channel change in experimental braided streams. For each alluvial river system, we assembled a time series of channel maps K_β , in which K represents the channel map binary matrix and β is an integer that represents the time step. We then selected each channel map in turn to be the baseline channel map (K_B). We differenced each baseline channel map with a corresponding time series of “transient” channel maps, K_T , picked such that $T \geq B$. The absolute values of these differences were summed across rows (m_r) and columns (n_c) to obtain the number of changed pixels, D , between each baseline-transient channel map pair.

$$D(B, T) = \sum_{i=1}^{m_r} \sum_{j=1}^{n_c} |K_B - K_T| \quad (1)$$

We then scaled this difference against the number of changed pixels that would be observed by randomly scattering the same proportions of wet and dry pixels across the fluvial surface. This random scatter parameter, Φ , is:

$$\Phi = (f_{w,B} \cdot f_{d,T} + f_{d,B} \cdot f_{w,T}) \quad (2)$$

where f is “fraction”, subscript w is “wet” (channel), and subscript d is “dry” (unoccupied fluvial surface). We used Φ to compute a normalized overlap (O_Φ) in channel position between time steps B and T . A value of 1 for O_Φ indicates that the two channel maps are identical, and a value of 0 indicates that the two channel maps have an amount of overlap indistinguishable from random noise. Negative values indicate that there is less overlap between the channel maps than would be expected of samples of random noise.

$$O_\Phi = 1 - \left(\frac{D}{A \cdot \Phi} \right) \quad (3)$$

A is the area of the fluvial surface in pixels. O_Φ is calculated for each $K_B - K_T$ pair because the proportions of observed “wet” and “dry” pixels were not constant through a data

set, although they tended to be normally distributed about a mean (Figure 4).

Each channel overlap time series is given relative to its baseline channel position occurring at $t = 0$. We superposed all of these time series to yield a better statistical picture of the time evolution of each channel system. We thus assumed that all of these systems are statistically stationary. This is reasonable so long as the mean external conditions (water and sediment discharge, bed and bank material, mean channel slope) remain the same in a time-averaged sense. We tested for stationarity by applying an augmented Dickey–Fuller test [Dickey and Fuller, 1979, 1981] to our instantaneously-measured rates of channel planform change. With a single lag, all experiments exhibited statistical stationarity ($p < 0.001$). With multiple lags, the results of the augmented Dickey–Fuller tests were indistinguishable from the same tests performed on Gaussian white noise with time series lengths, means, and standard deviations derived from each of the experimental time series. To test for long-range trends, attempted a linear fit to each instantaneous planform change time series. Here, all line slopes were near 0, the median R^2 value was 0.0050, and the maximum R^2 value was 0.0472; these values likewise indicate statistical stationarity.

3.2.2. Reworking of the fluvial surface

To calculate a time scale over which the fluvial surface is reworked, we first picked a single baseline channel map (K_B) as above. Then we selected from the fluvial surface area matrix (F) only those pixels that were not occupied by channel at the baseline time step, as these constitute the region available for new channel occupation, and called this matrix F'_B .

$$F'_B = F - K_B \quad (4)$$

Because the initial channel area was subtracted from F to create F'_B , the total relevant pixel area decreases accordingly by a factor of $f_{d,B}$.

$$\sum_{i=1}^{m_r} \sum_{j=1}^{n_c} F'_B = A \cdot f_{d,B} \quad (5)$$

We summed the series of channel maps K'_{B+1} through K'_T for each time step $\beta = T$ after the baseline time step. Here, the primes indicate that these channel maps have had the initial channel area removed from the analysis according to their respective modified fluvial surface mask, F'_B . This summed K'_{B+1} through K'_T matrix gives the total number of times each pixel has been occupied between time steps $\beta = B+1$ and $\beta = T$. We then counted the number of zeros (unreworked pixels: $N'_{B,T}$) in this matrix at each time step T corresponding to each baseline time step B :

$$N'_{B,T} = \sum_{i=1}^{m_r} \sum_{j=1}^{n_c} \left[\left(\sum_{\beta=B+1}^T K'_\beta \right) \equiv 0 \right] \quad (6)$$

We then divided this sum by the observed area, $A \cdot f_{d,B}$, to obtain the fraction of not initially occupied fluvial surface that has been reworked, f_R .

$$f_R = 1 - \frac{N'_{B,T}}{A \cdot f_{d,B}} \quad (7)$$

We overlaid all of the f_R measurements onto a common relative-to-baseline time axis by setting $t = 0$ at each baseline time-step as we do to measure loss of planform overlap (Section 3.2.1).

3.2.3. Instantaneous channel planform change

Our third measure of river channel mobility is the rate of channel planform change, measured as the amount of surface area reworked per unit time. For a single-thread stream, this is equivalent to the migration rate integrated down the

length of the channel plus the avulsion magnitude (areal extent) times its frequency.

While it would be simplest to difference channel maps at adjacent time steps, the color-based technique of separating channels from unchannelized fluvial surface produces minor inconsistencies in the area that is classified as “channel” due to very small changes in (1) lighting and dye concentration (Section 3.1) and (2) channel depths in the braided systems that allow portions of them to fluctuate across the channel map dye intensity threshold. This noise would cause too much planform change to be measured between adjacent time steps, so we filter it out with a technique known as double differencing, which is commonly applied to remove noise from GPS data [e.g., Alber et al., 2000]. Noise in the channel maps occurs at a similar magnitude in all nearby time steps, so approximately the same amount of additional loss of overlap due to random noise, given by the independent and identically distributed random variables X_1 and X_2 , is observed between K_{B+2} and K_B , and K_{B+1} and K_B . In addition, the channel maps are recorded at a high enough temporal resolution that the channels move at very close to the same velocity during closely-spaced time steps. These two properties permit us to cancel out the component of observed change that is due to the noise in the channel maps by subtracting the two differences, $(K_{B+2} - K_B)$ and $(K_{B+1} - K_B)$, from each other.

$$\begin{aligned} D(B+1) &= \sum_{i=1}^{m_r} \sum_{j=1}^{n_c} |K_B - K_{B+1}| \\ &= \left[\sum_{i=1}^{m_r} \sum_{j=1}^{n_c} |K_B - K_{B+1}| \right]_{cc} + X_1 \end{aligned} \quad (8)$$

$$\begin{aligned} D(B+2) &= \sum_{i=1}^{m_r} \sum_{j=1}^{n_c} |K_B - K_{B+2}| \\ &= \left[\sum_{i=1}^{m_r} \sum_{j=1}^{n_c} |K_B - K_{B+2}| \right]_{cc} + X_2 \end{aligned} \quad (9)$$

$$\begin{aligned} D(B+2) - D(B+1) &= \left[\sum_{i=1}^{m_r} \sum_{j=1}^{n_c} |K_B - K_{B+2}| - |K_B - K_{B+1}| \right]_{cc} \\ &\quad + [(X_2 - X_1) \rightarrow 0] \\ &= \left[\sum_{i=1}^{m_r} \sum_{j=1}^{n_c} |K_{B+1} - K_{B+2}| \right]_{cc} + [(X_2 - X_1) \rightarrow 0] \end{aligned} \quad (10)$$

$$\text{for } T - B \ll \tau_M : \quad (11) \\ D(B+2) - D(B+1) \approx \left[\sum_{i=1}^{m_r} \sum_{j=1}^{n_c} |K_B - K_{B+1}| \right]_{cc}$$

Here, the subscript cc denotes the difference between the channel maps due only to actual river channel motion, and τ_M is a characteristic planform overlap time scale that is much greater than the time scale for which instantaneous measurements of channel motion must be made (see Section 7.3).

In the planform overlap analysis we counted areas subject to both erosion and deposition. To obtain only a bank

erosion rate for the experiments, we assumed that long-term lateral erosion and deposition were equal, which is consistent with our measurements of on-average channel area with time (Figure 4). This allowed us to divide our double differenced result by 2 to obtain a rate of instantaneous channel motion in pixels per time step. We then converted these numbers into fractional areal change per unit time by dividing the observed pixel area reworked by the full fluvial surface area, A , and the time $\Delta t_{B+1,B+2}$ that elapsed between the two time steps being studied. The resulting rate, $\dot{\zeta}_f$, has units of [1/time]. Because it has no spatial units, it can be interpreted as a rate of fractional planform change over the whole fluvial surface or as an on-average rate of lateral motion across a given cross-section.

$$\dot{\zeta}_f = \frac{D(B+2) - D(B+1)}{2A\Delta t_{B+1,B+2}} \quad (12)$$

We compiled this value for each double differenced time step pair.

4. Curve Fitting

We fit curves to our observations of channel planform change to generate a minimal set of parameters that describe our measurements of these river systems and allow us to make some inferences about the relationships between them. Table 3 is a compilation of the parameters for the curve fits that are described in this section. These include loss of channel planform overlap (M), fluvial surface reworking (R), and rates of fractional planform change per unit time ($\dot{\zeta}_f$). The curve fits are shown in Figures 5 and 6.

4.1. Planform Overlap

The change in overlap with the original planform over time takes the rough form of an exponential decay (Figure 5), which can be described by the equation

$$O_\Phi = (a_M - p_M) e^{-Mt} + p_M \quad (13)$$

where the channel mobility parameter M is the decay constant. M describes how quickly the channel system reconfigures itself. The channel preference parameter, p_M , is the asymptote that gives the fraction of the observed area that the channel never touches. The third parameter, a_M , is the y-intercept. It is made a free parameter here to be a correction factor due to the artificially-high measured loss of overlap between the first and second time steps, as described in Section 3.2.3.

The parameter p_M is zero when the river channel(s) move freely across the observed area, and is greater than zero when the channel(s) appear to prefer one part of the observed area more than another. In our study, this term is generally near zero but positive. It is near zero because we define the observed area to be the fluvial surface, across which the braided channels in noncohesive sediment that dominate all but the vegetated BV-2 experiment freely moved. It is positive because in the delta experiments [Kim et al., 2006a, b; Sheets et al., 2007; Martin, 2007], a channel always existed immediately downstream of the sediment and water point source, and in the braiding-vegetation experiment [Tal and Paola, 2007, 2010] the channel system remained close to the wall along some portions of the fluvial surface for long periods of time. Even with careful experimental design, boundary conditions typically exert some influence on channel form.

4.2. Reworking of the Fluvial Surface

The amount of unreworked fluvial surface decays exponentially with time (Figure 6). This exponential decay can be described in a form identical to that for loss of planform

overlap

$$1 - f_R = (a_R - p_R) e^{-Rt} + p_R \quad (14)$$

where f_R is the fraction of the total surface area that has been visited by the flow, not including the area initially occupied by the channel, and R is the decay constant for fluvial surface reworking (also called the reworking rate). The terms a_R and p_R are analogous to a_M and p_M , respectively, in Section 4.1. p_M is positive if there are areas on the fluvial surface that the channel preferentially does not visit. The term a_R is a necessary y-intercept correction factor due to the image analysis. Sudden increases in observed channel area, for example due to changes in lighting, cause a small but sudden spike in the amount of area observed to be reworked, especially around $t = 0$ when the entire fluvial surface area is open to this artificial reworking.

The fluvial surface reworking data (Figure 6) display less scatter than the channel planform overlap data (Figure 5). The scatter in the overlap data reflects the fact that even if a channel system “forgets” its initial channel pattern, it will at times overlap it more than at others, resulting in large spikes in the measured O_Φ . Because we cycle through baseline time steps, these data form a large point cloud around the asymptote. In our reworking analysis, once-reworked regions cannot be reworked again, resulting in a significantly tighter point cloud about the asymptote.

4.3. Instantaneous Channel Planform Change

The simplest way to calculate channel planform change per unit time would be to take an average of the instantaneous planform change (defined in Section 3.2.3) divided by the time elapsed between each pair of observations. As a few outliers exist (caused, for example, in BV by moving the calibration dye trays and not by river dynamics), we un-weighted these outliers to calculate rates of real channel motion (Table 3). These direct measurements of fractional planform change $\dot{\zeta}_f$ were then multiplied by mean fluvial surface widths to obtain rates of average channel lateral mobility across a cross-section in meters per hour ($\dot{\zeta}$, Table 2).

5. Linking Measurements across Time Scales

All three of our measurement methods are fundamentally linked to channel mobility. By the definition of a derivative, $\dot{\zeta}_f$ is the change in channel position as a fraction of the fluvial surface area as Δt , the time between measurements, $\rightarrow 0$. Loss of planform overlap and fluvial surface reworking are described by exponential functions, so their derivatives at $t = 0$ are linear functions of the decay constants M and R , respectively. This convergence at $t = 0$ means that $\dot{\zeta}_f$, M , and R , must be linearly related to one another.

We investigated this relationship by comparing measured time scales for loss of planform overlap and fluvial surface reworking with characteristic time scales that use the instantaneous rate of channel position fractional change, $\dot{\zeta}_f$. We defined an idealized channel time scale, $\tau_{ch,M}$ [modified from Jerolmack and Mohrig, 2007], to compare with measured loss of channel system overlap, and an idealized fluvial surface time scale, $\tau_{fs,R}$, to compare with measured fluvial surface reworking.

$$\tau_{ch,M} = \frac{f_w(1 - (\bar{\Phi}/2))(1 - O_\Phi)}{\dot{\zeta}_f} \quad (15)$$

$$\tau_{fs,R} = \frac{\bar{f}_d f_R}{\dot{\zeta}_f} \quad (16)$$

Here, $\bar{\Phi}$ is the time-averaged value of Φ for the experiment. The channel time scale is that required for a channel to move monotonically in one direction a distance that would cause it to have a spatial correlation of O_Φ . The fluvial surface time scale likewise is that required for a channel to rework a fraction f_R of \bar{f}_d , the average fraction of the fluvial surface that is not initially occupied by the channel, without reoccupying any already-reworked area (i.e. with perfect efficiency). These time scales therefore represent the shortest amount of time it could possibly take a channel moving at a known rate to lose overlap with itself or rework the fluvial surface.

We compared these characteristic time scales with measured n - e -folding times τ_M and τ_R , where n is the number of integer exponential decay times ("e-folds") measured for the channel system:

$$\tau_M = \frac{n}{M} \quad (17)$$

$$\tau_R = \frac{n}{R} \quad (18)$$

When substituting n e-folds for the amount of lost planform overlap ($1 - O_\Phi$) in Equation 15 and the fraction of reworked fluvial surface (f_R) in Equation 16, we obtain:

$$\tau_{ch,M} = \frac{f_w(1 - (\bar{\Phi}/2))(a_M - p_M)(1 - e^{-n})}{\dot{\zeta}_f} \quad (19)$$

$$\tau_{fs,R} = \frac{\bar{f}_d(a_R - p_R)(1 - e^{-n})}{\dot{\zeta}_f} \quad (20)$$

The ratios between the measured times and the characteristic time scales are:

$$\frac{\tau_M}{\tau_{ch,M}} = \left(\frac{\dot{\zeta}_f}{f_w M (1 - (\bar{\Phi}/2))(a_M - p_M)} \right) \left(\frac{n}{1 - e^{-n}} \right) \quad (21)$$

$$\frac{\tau_R}{\tau_{fs,R}} = \left(\frac{\dot{\zeta}_f}{\bar{f}_d R (a_R - p_R)} \right) \left(\frac{n}{1 - e^{-n}} \right) \quad (22)$$

The first term on the right hand side of Equation 22 combines the important quantities in determining the ratio of the measured fluvial surface reworking time to the shortest possible reworking time. Because the measured time scale (τ_R , Equation 18) increases linearly with n while the e -folding time scale ($\tau_{fs,R}$ Equation 20) increases as $-e^{-n}$, the ratio between the two is a function of the chosen time scale. This satisfies the expectations of the behavior of the equations in the limits: As $f_R \rightarrow p_R$, $n/(1 - e^{-n}) \rightarrow \infty$, and therefore $\tau_R/\tau_{fs,R} \rightarrow \infty$, following the asymptote in Equation 14. As $f_R \rightarrow 0$, $n/(1 - e^{-n}) \rightarrow 1$ and therefore $\tau_R/\tau_{fs,R} \rightarrow \dot{\zeta}_f / (\bar{f}_d R (a_R - p_R))$. In theory, $\tau_R / (\bar{f}_d R (a_R - p_R))$ should be unity, because over very short time periods, the river channel will be able only to move away from its original position and will not be able to rework previously-reworked fluvial surface area, thereby making the instantaneous and long-term reworking rates be equal. This can be shown rigorously by solving the time derivative of Equation 14 at $t = 0$ while knowing that at $t = 0$, any channel motion ($\dot{\zeta}_f$) can only rework previously-unvisited parts of the fluvial surface, or more simply by taking $n = 0$ in Equation 20:

$$R = \frac{\dot{\zeta}_f}{f_d(a_R - p_R)} \quad (23)$$

The same logic applies for loss of planform overlap (Equation 19):

$$M = \frac{\dot{\zeta}_f}{f_w(1 - (\bar{\Phi}/2))(a_M - p_M)} \quad (24)$$

Equations 23 and 24 allow us to remove the first terms from the right hand sides of Equations 21 and 22; this sets them

equal both to each other and to the ratio of linear and exponential time scales in the second term on the right hand side:

$$\frac{\tau_M}{\tau_{ch,M}} = \frac{\tau_R}{\tau_{fs,R}} = \frac{n}{1 - e^{-n}} \quad (25)$$

As a reasonable approximation of complete loss of planform overlap and fluvial surface reworking, we choose a 3- e -folding time, which corresponds to 95% loss of overlap and reworking.

$$\left. \frac{\tau_R}{\tau_{fs,R}} \right|_{n=3} = \left. \frac{\tau_M}{\tau_{fs,M}} \right|_{n=3} = 3.16 \quad (26)$$

Figure 7 shows that most of the data points lie near the theoretical $\tau_R/\tau_{fs,R} = 3.16$ line, in accordance with expectations. There are, however, two marked deviations. First, channels in the braided system, BV-1, move rapidly but do not lose overlap with their original positions or rework their fluvial surface as quickly as would be predicted. This suggests that while BV-1 rapidly moves bars, it maintains a more persistent and longer-lived self-similarity. Second, the measured reworking rate in DB03-2 is barely any slower than the most rapid possible (Equation 16) reworking rate. Its subcritical flow causes ripples to develop pervasively throughout the channels [Martin, 2007], roughening them and pushing the channels more rapidly across the fluvial surface (see Section 6.5). The grouping of all of the other data around 3.16 implies that it may be possible to use short-term measurements of channel motion ($\dot{\zeta}_f$) to predict longer-term rates of channel planform change and fluvial surface reworking.

6. Measured Channel Mobility and Fluvial System Forcings

6.1. Theory

River channel lateral motion in a given cross-section ($\dot{\zeta}$ [m/hr]) is a combination of channel migration rate ($\dot{\zeta}_{\text{mig}}$) and avulsion magnitude times frequency ($\dot{\zeta}_{\text{av}}$).

$$\dot{\zeta} = \dot{\zeta}_{\text{mig}} + \dot{\zeta}_{\text{av}} \quad (27)$$

Because the experimental systems exhibited only depositional avulsions (i.e. those avulsions that are caused by aggradation of the bed and superelevation of the channel), we chose a channel superelevation criterion for the frequency of avulsion, following Jerolmack and Mohrig [2007] [see also Bryant *et al.*, 1995; Mohrig *et al.*, 2000]. This avulsion frequency is the reciprocal of the time required for the channel to aggrade (aggradation rate $\dot{\eta}$) to a full channel depth (mean channel depth \bar{h}). The magnitude of an avulsion is equal to the total channel width (i.e. all threads) in a cross-section; for this, we use the mean width, \bar{b} .

$$\dot{\zeta}_{\text{av}} = \bar{b} \frac{\dot{\eta}}{\bar{h}} H(0) \quad (28)$$

$H(0)$ is the Heaviside function, defined to be 1 for $\dot{\eta} \geq 0$ and to be 0 otherwise; this is to exclude the case of an "anti-avulsion" with negative channel planform change as the channel incises. When calculating $\dot{\eta}$ on the deltas, we assumed that delta surface aggradation rate matched the rate of base level change (i.e. sea level rise plus subsidence). For rivers in the field, direct measurements of in-channel aggradation rates would be used instead.

Channel lateral migration is the morphologic equivalent to a flux of sediment in a cross-stream (y) direction. Whatever the cause of the lateral movement of sediment, we hypothesize that the lateral sediment flux (i.e. channel migration) should increase with increasing downstream sediment

transport. More formally, the downstream sediment flux, $q_{s,x} = q_s$ [m/s] (the x direction of transport being generally implied), should be proportional to the cross-stream sediment flux $q_{s,y}$, which is the channel lateral migration rate $\dot{\zeta}$ times one minus the porosity: $q_{s,y} = \dot{\zeta}_{\text{mig}}(1 - \lambda_p)$. In order to be dimensionally consistent, this relationship must be linear by a constant of proportionality, Ξ . We measured downstream sediment discharge, Q_s [m^3/s], as the sediment input to the deltas and the sediment output from the braided-vegetated systems. This difference is because the deltas are depositional systems for which we use sediment input as a characteristic discharge, while sediment discharge in an inland system is best measured as the throughput, not the input. We used mean channel width, \bar{b} [m], and mean flow depth, \bar{h} [m], to calculate sediment flux as $q_s = Q_s/(\bar{b}\bar{h})$:

$$\dot{\zeta}_{\text{mig}} = \Xi \frac{q_s}{(1 - \lambda_p)} = \Xi \frac{1}{(1 - \lambda_p)} \frac{Q_s}{\bar{b}\bar{h}} \quad (29)$$

Beard and Weyl [1973] showed experimentally that $\lambda_p = 0.39$ for well-sorted wet-packed sand at 120 and 500 microns (i.e. the sizes that were used in the experiments; see Table 2). Since the bed and banks were made of the same material in these experiments, we do not need to worry about the complications of grain size or material property heterogeneity. All of the material moves as bed load, also freeing us from complications resulting from multiple modes of sediment transport. As such, these experiments provide a data-rich and simplified testing ground for our hypothesis that sediment flux controls channel lateral mobility.

Equation 29 is a morphodynamic sediment transport relationship [e.g., *Popov*, 1962a, b; *Neill*, 1971; *Church*, 2006] that relates channel planform change to bed material transport as observed via the evolution of the channel. Analogous relations relating sediment transport to bedform evolution are presented by *McElroy and Mohrig* [2009].

With this morphodynamic relationship for channel lateral migration, we rewrite Equation 27 in more concrete terms:

$$\dot{\zeta} = \Xi \frac{1}{(1 - \lambda_p)} \frac{Q_s}{\bar{b}\bar{h}} + b \frac{\dot{\eta}}{\bar{h}} H(0) \quad (30)$$

Our constant of proportionality, Ξ , captures other factors that affect channel migration rates. Bank stabilization by vegetation or consolidated bank materials should inhibit channel migration and decrease Ξ [e.g., *Simon and Collison*, 2002; *Pollen and Simon*, 2005; *Constantine et al.*, 2009; *Güneralp and Rhoads*, 2011]. Channel curvature, on the other hand, increases the lateral variability of channel velocities, bed shear stress, and therefore sediment transport capacity [Hooke, 1975]; this should enhance channel migration rates [e.g., *Furbish*, 1988; *Güneralp and Rhoads*, 2010] and therefore also increase Ξ . This parameterization is consistent with the work of *Howard and Knutson* [1984], who posited that lateral migration rates are controlled by a combination of bank erodibility and sediment discharge.

6.2. Sediment Flux Controls Channel Mobility

Figures 8.A and 8.B show a correlation between channel mobility and sediment flux on both dimensional (Figure 8.A) and dimensionless (Figure 8.B) axes. If all of these experiments were identical, and therefore had the same value of Ξ , we predict that the relationship between their dimensional forms would be linear. While these data are from very disparate systems, they do approximate an increasing trend because the 2.5 order of magnitude range in sediment flux outweighs the one order of magnitude variability in Ξ . Independently from but simultaneously with our laboratory investigations, *Dunne et al.* [2010] used field observations and numerical modeling to show that increased sediment supply forces more rapid channel motion, and future laboratory, computer, and field work should help to

better understand the mechanics behind these observations. Figure 8.B is a dimensionless version of this relationship between sediment transport and channel mobility that uses common input variables for experimental studies: grain size (D) and sediment-to-water ratio (Q_s/Q). A combination of this graph and the calculated values of Ξ for each experiment (Table 2) therefore constitute a set of predictions of channel mobilities that can be tested and expanded experimentally.

Figure 8.C shows that there is little relationship between channel mobility and our aggradational avulsion criterion in the experimental deltas, even with a wide range of aggradation rates. That XES02 (circles) shows no relationship between lateral mobility and aggradation rate is particularly important to this point: in this experiment, aggradation rate was controlled primarily by base level fluctuations and did not covary with sediment input (as it did for DB03-1 and DB03-2). Further, XES02 follows the trend of the other experiments in Figures 8.A and 8.B, supporting a stronger sediment flux control. This contradicts expectations of increased channel mobility with increased superelevation-driven avulsion frequency (Equation 29) [Mohrig et al., 2000; Jerolmack and Mohrig, 2007] (Section 6.2), and is likely due to the noncohesive sediment that allows the channels to migrate much more rapidly than they move by avulsion.

6.3. Base Level Rise and Avulsion Promote Fluvial Surface Reworking

While sediment flux controlled the rate at which channels moved laterally, avulsions helped to facilitate more rapid fluvial surface reworking. Aggradation, often linked to deltaic lobe deposition, lead to channel back-filling and caused channels to superelevate and avulse [Bryant et al., 1995; Mohrig et al., 2000] to unoccupied regions of the delta surfaces. This and analogous situations have been observed in field studies [e.g., *Frazier*, 1967; *Roberts*, 1998], laboratory experiments [e.g., *Sheets et al.*, 2007; *Martin et al.*, 2009; *Powell et al.*, 2012; *Reitz and Jerolmack*, 2012], and numerical models [e.g., *Overeem et al.*, 2005] of deltas.

Figure 8.D shows fluvial surface reworking rate (R) vs. avulsion magnitude times frequency ($\dot{\zeta}_{\text{av}}$). Some variability in reworking rate occurred with little or no depositional avulsion forcing. This scales with increasing sediment flux: in the absence of avulsions, sediment-flux-induced channel mobility lead to more rapid reworking. Where avulsions did occur, they increased the rate of fluvial surface reworking by rapidly moving the channel to unoccupied portions of the fluvial surface, thereby reworking the new channel footprint and facilitating channel migration into hitherto-unouched regions.

XES02 experienced base level changes that we compare in Figure 9 with our channel overlap (M) and fluvial surface reworking (R) decay constants. These data show that rates of fluvial surface reworking and loss of planform overlap increase with base level rise. While rates of fluvial surface reworking are significantly higher for the base level rise phases of XES02 than they are for the base level fall phases, rates of loss of planform overlap are roughly constant throughout, as these are tied more closely to local channel migration. A “relative reworking efficiency”, calculated as a ratio of the reworking and overlap rates, shows that with increasing base level rise the reworking rate increases much faster than the rate of loss of channel planform overlap. This provides further evidence that rivers that move laterally by avulsive channel redistribution rework their fluvial surface more rapidly than systems that move laterally at the same rate (i.e. the same $\dot{\zeta}_f$) but by lateral migration.

6.4. Vegetation

Lateral migration rates for the steady state braided and vegetated channel systems were 1.56 and 0.09 meters per

hour, respectively: the addition of vegetation caused a 17-fold reduction in channel migration rate. Our measured migration rate for the vegetated case is lower than that reported by *Tal and Paola* [2010] because we smoothed the data to remove noise (Section 3.2.3), which exists on the fringes of these channels where the dye intensity is close to our threshold. In spite of this 17-fold decrease in channel migration rate, Ξ decreased only by a factor of 2.6. This disparity indicates that the majority of the reduction in channel migration rate was due to a combination of deeper channels and lower sediment transport capacity—likely from the mechanical strength and additional roughness of the vegetation. The 2.6-fold change in Ξ can be attributed to a combination of changes in channel geometry and flow fields as the system became single-thread, and the greater difficulty of detaching sediment from the vegetated banks. This shows that vegetation and vegetation-induced bank cohesion produce a combined influence on channel lateral mobility by changing channel geometry, channel roughness, and grain detachment potential.

The fraction of the fluvial surface that was actively reworked, $1 - p_R$, dropped from 79% to 17% as the addition of vegetation confined the flow [consistent with the observations of *Tal and Paola*, 2007, 2010]. Within these differently-sized areas, the fluvial surface reworking rate (R) and rate of loss of channel planform overlap (M) were approximately the same for both the vegetated and unvegetated stages of the experiment. This shows that while vegetation confined BV-2 to a narrower corridor, both braided and single-thread rivers share a common bar reconfiguration time scale.

6.5. Channel Patterns and Bed Topography

In BV-1, Ξ is unity, meaning that the barforms moved at the same rate as the bed material. This implies that all of the sediment passing through this system interacted with the bars, corroborating the work of *Pyrcz and Ashmore* [2003], who show that sediment path lengths in experiments are given by the pool-bar spacing. This lends additional support for the often-used morphological (or morphodynamic) method of estimating sediment transport in braided streams in the field [e.g., *Church*, 2006], in which the observed motion of barforms is inverted to obtain rates of bed material transport.

This full sediment interchange with the bed was not observed in the experimental deltas. Here, values of Ξ are much lower, and much of the sediment passed directly through these systems to build deltaic lobes. We attribute this largely to the shorter transport distance on the deltas: these were 1–4 m long, compared with the 16 m long BV-1 and BV-2, and this distance is too short for flow divergence and re-convergence around barforms (2–3 m long in BV-1) and significant barform migration to occur.

DB03-2 was built with a very low surface slope to permit $\mathbf{Fr} < 1$ flow. This subcritical flow over a sandy bed formed ripples with heights that were a large fraction of the flow depth and acted as “bars” (at a smaller scale than those in BV-1) to steer the channel [*Martin*, 2007]. This combination of low downstream gradients and self-forming in-channel topographic variability and roughness caused the channel to be self-repelling and very rapidly rework its whole fluvial surface: its 3-e-folding reworking time is barely longer than it would take an ideally efficient channel to wipe across the fluvial surface from one side to the other (Figure 7; see Equation 16). Ξ for DB03-2 is almost four times Ξ for its sister experiment, DB03-1, that had supercritical flow. This represents a fourfold increase in sediment exchange with the fan surface.

Increased sinuosity along a reach of BV-2 correlates with more rapid planform change (Figure 10). This is consistent

with research on meander bends [e.g., *Hooke*, 1975; *Furbish*, 1988, 1991; *Güneralp and Rhoads*, 2009, 2010; *Parker et al.*, 2011], which shows that channel curvature sets up a situation in which sediment deposits on the inner bank and erodes from the outer bank, thereby further enhancing the sinuosity of the channel. This is not a runaway process, however, and increases in sinuosity beyond a radius of curvature to width ratio of ~ 3 [*Hickin and Nanson*, 1975; *Nanson and Hickin*, 1983]) lead to decreased meander migration rates.

7. Discussion

7.1. Normally Distributed Channel Widths

Channel widths, as obtained from wetted area in our channel maps, are normally distributed about the mean (Figure 4). These normal distributions support the concept of an equilibrium alluvial channel width [*Parker*, 1979; *Parker et al.*, 2011], in which deviations from the mean width are allowed, but are unstable and brought back to equilibrium by erosion of and/or deposition on the banks due to increased wall shear stresses in narrower channels and decreased wall shear stresses in wider channels.

Figure 4 shows histograms of channel width normalized to mean width. We observe the greatest standard deviations in normalized channel width for the deltas, which experienced repeating cycles of (1) channelization and lobe building and (2) sheetflow and searching for a new region to channelize. In the braided-vegetated dynamics experiment, this standard deviation dropped significantly with the addition of vegetation. This indicates that the width of the deeper single-thread channel in BV-2 is more stable than the width of the braided channels, as expected, and suggests that there exists a strong coupling between point bar deposition and cut bank erosion that maintains this enhanced stability [cf. *Parker et al.*, 2011].

7.2. Exponential Decay in Reworking

The exponential decay functions used to model fluvial surface reworking imply that channel positions are independent of their previous positions. This is physically reasonable for highly-avulsive aggrading fan delta experiments, in which the fans maintain a symmetrical shape with subtle surface topography. Prograding deltas, on the other hand, have been shown to persistently reoccupy certain positions [*Reitz et al.*, 2010, Figure 3] because topographic signatures of past channel occupation are not erased by channel burial as they are in our often-aggradational experiments.

While our exponential decay curves provide good fits to our data with few free parameters, they are not perfect and the complex feedbacks between flow, sediment transport, and landscape morphology may preclude the ability to understand any but the simplest landscapes with a single function. Near the maximum runtimes of many of the experiments, our exponential curves for fluvial surface reworking approach their asymptotes, p_R , and start to underpredict the amount of reworked fluvial surface (Figure 6). Although the data become sparse at long time intervals, making interpretations more tenuous, this deviation could indicate a slower process of river channel planform change that is superimposed on the exponential function. We hypothesize that the exponential functions are good indicators of fluvial surface reworking due to bar and bank migration within the river corridor and avulsions that move the location of the river corridor. The remaining unworked areas are often high terraces, which can be reworked only when the a channel comes into contact with their edges—a much lower probability occurrence than the river channel coming into contact with one of its bars. Our longest-running experiment, DB03-2, had a surface with no terrace regions due to

its ripple-forced rapid channel motion (Section 6.5), and almost completely reworked its surface (asymptote $p_R = 0.3\%$ unworked). The exponential function for DB03-2 fits its data without the overpredictive discrepancy that characterizes all of our other experiments that approach their reworking asymptotes. Additional long-term experiments would help us to further characterize the long-term statistics of fluvial surface reworking.

7.3. Measurement Frequency

Our measured loss of channel planform overlap with time can be viewed as a measurement of rates of channel planform change over various time scales of averaging. When measurements are spaced closely relative to a channel migration rate, there is little risk of error in interpolating between the channel positions at two different times. Over longer measurement intervals, part of a channel may leave its old position and then return, reducing the measured amount of river channel planform change. In the longest term, we see the measured loss of planform overlap reach an asymptote (Figure 5) that is often near the amount of overlap expected for two random sets of channel and unchannelized fluvial surface. This saturation in loss of planform overlap has also been noted in experiments by *Sapozhnikov and Foufoula-Georgiou* [1997]. The observation that apparent rates of change decrease with measurement time scale may help to resolve the discrepancy that *Hooke* [1980] noticed in that short-term field measurements showed more rapid alluvial channel migration than did measurements from historical maps spanning 135 years (1840 to 1975).

7.4. Channel Mobility and Fluvial Stratigraphy

The relationship between channel mobility (as avulsions) and preserved channel strata was first developed by *Leeder* [1978]. Our approach to measuring channel mobility can be used to formulate a simple relationship between fluvial surface reworking rates and bulk volumes of channel and overbank deposits (i.e. the net to gross ratio for reservoir rock) preserved in the stratigraphic record:

$$f_{ch} = f_w + \bar{f}_d (1 - p_R) \left[1 - \exp \left(-R \frac{\bar{h}}{\eta_{ob}} \right) \right] \quad (31)$$

Here, f_{ch} is the fraction of the deposit volume that is channel deposit, f_w is the wetted (channel) fraction, $\bar{f}_d = (1 - f_w)$ is the dry (not channel) fraction, p_R is the reworking asymptote, \bar{h} the mean channel depth, and η_{ob} is the mean overbank aggradation rate, which we approximate as sea level rise plus subsidence (a reasonable estimate for the aggradational effects of shallow flow in these experiments). This equation states that the volume of channel deposit is given by the planview fractional area of the channel, plus the fractional area reworked over the time required for overbank deposition to raise the mean surface level by one scour depth such that these deposits are protected from further erosion and reworking by the channel. Because of our spatially-dimensionless (fluvial surface normalized) approach in calculating fluvial surface reworking (R [1/hr]) and channel area (f_w [-]), our deposit “volumes” can apply equally to 3D deposits, cross-sections, or single cores; we find a strike section to be easiest to visualize. We assume that the stratigraphy is composed of a bimodal distribution of channel and overbank deposit. Therefore

$$\eta_{ob} = 1 - f_{ch} \quad (32)$$

where η_{ob} is the overbank deposit fraction. The endmembers of the set of Equations 31 and 32 are that no overbank deposit is produced when $\eta_{ob} \rightarrow 0$ and/or when $R \rightarrow \infty$, and that one channel-width of channel deposit remains as $\eta_{ob} \rightarrow \infty$ and/or $R \rightarrow 0$.

We test this model with DB03-1 and DB03-2 by comparing predicted and observed fractions of channel deposit.

Martin [2007] measured ~60% channel deposit in DB03-1 and ~95% channel deposit in DB03-2 by slicing the experimental deltas and measuring stratigraphy. Equation 31 gives 72% channel deposit in DB03-1 and 99% channel deposit in DB03-2, reproducing the observed trend. The fact that we overshoot in both cases is likely because only a portion of the measured channel area that we use to calculate reworking rates actually produces the deep scours preserved in the stratigraphy. With additional work and refinement, and especially with the application of cross-sectional and three-dimensional topographic data, these principles may help to translate between channel mobilities and channel deposit fractions in fluvial deposits.

8. Conclusions

We create an area-based methodology to measure instantaneous rates of channel planform change, loss of channel system planform overlap, and fluvial surface reworking. We develop these metrics using a variety of laboratory experiments that in turn provide new insights into (1) the relationships between time scales of fluvial system evolution and (2) response of channel systems to external forcings. Our major contributions are that:

1. We have developed functional relationships that connect river channel lateral mobility from short-term measurements to long-term loss of planform overlap and fluvial surface reworking (Section 5). Fluvial surface reworking rates can be used in turn to connect surface processes to fluvial stratigraphy (Section 7.4). In alluvial systems, the present and the past are the keys to one another.

2. Channel mobility is driven primarily by sediment flux, with bank stabilization by vegetation decreasing it, and irregularities in channel bed and planform geometry (ripples and sinuosity, respectively) increasing it. Aggradationally-forced depositional avulsions correlate poorly with channel mobility, but well and positively with fluvial surface reworking rates, indicating that they act to distribute the channel system more efficiently across the whole fluvial surface. All of the sediment passing through BV-1, the braided experiment, is incorporated into migrating barforms. This means that its sediment flux and barform migration rate are identical, and lends laboratory support for morphodynamic methods of measuring sediment transport rates.

In addition to these, we show that:

1. Channel widths are normally distributed with time, implying that they are stable with constant forcings on the fluvial system.

2. Saturation in loss of planform overlap with time can explain reduced rates of observed channel mobility with longer intervals between observations.

We are able to explain channel response to forcings (vegetation, sediment flux, aggradation, and planform geometry) and relationships between rates of channel planform change as measured across multiple time scales in these experimental settings. This bodes well for our ability to better understand the evolution of alluvial systems through time.

Notation

- F fluvial surface area matrix (1 = fluvial surface; 0 = regions outside the fluvial surface).
- β time step [hr].
- K_β channel map binary matrix at time step β (1 = “wet”; 0 = “dry”).
- B baseline time step; plotted at time $t = 0$.

T	transient time step; these go from each baseline time step to the end of each experiment.
t	time since baseline [hr].
D	number of pixels that changed from “wet” to “dry” or “dry” to “wet” between two channel maps.
m_r	number of rows in matrix.
n_c	number of columns in matrix.
$f_{w,\beta}$	fraction of fluvial surface that is “wet” at time step β .
$f_{d,\beta}$	fraction of fluvial surface that is “dry” at time step β .
Φ	fraction of overlap observed between channel maps of randomly-distributed “wet” and “dry” pixels.
O_Φ	the amount of overlap between two channel maps, scaled to 1 for perfect overlap and 0 when overlap equals Φ (random noise).
A	fluvial surface area [pixels].
$'$	primes indicate reference to a baseline channel map in which the initial channel position is excluded from the analysis.
$N'_{B,T}$	number of unreworked pixels between time steps B and T .
f_R	reworked fraction of the fluvial surface.
$\Delta t_{\beta,\beta}$	time elapsed; two time steps (β) optionally specified [hr].
$\dot{\zeta}_f$	rate of channel planform change as fraction of total fluvial surface area [1/hr].
M	decay constant for rate of loss of channel planform overlap ($M \rightarrow$ “mobility”) [1/hr].
R	decay constant for rate of fluvial surface reworking; also called “reworking rate” [1/time].
a_M	y -intercept correction factor for loss of planform overlap.
a_R	y -intercept correction factor for fluvial surface reworking.
p_M	channel preference parameter: asymptote for the overlap analysis.
p_R	asymptote for the reworking analysis (i.e. fraction of fluvial surface never touched by channel).
n	number of e -folds.
$\tau_{ch,M}$	ideally efficient time scale for loss of channel planform overlap.
$\tau_{fs,R}$	ideally efficient time scale for fluvial surface reworking.
τ_M	measured time scale for loss of channel planform overlap.
τ_R	measured time scale for fluvial surface reworking.
$H(0)$	Heaviside function.
Ξ	Ratio of channel mobility to sediment flux: efficiency of sediment flux in driving channel planform change.
Fr	Froude number.
$\dot{\zeta}$	rate of channel planform change [m/hr].
$\dot{\zeta}_{\text{mig}}$	rate of channel planform change due to lateral migration [m/hr].
$\dot{\zeta}_{\text{av}}$	rate of channel planform change due to avulsion [m/hr].
b	channel width [m].

h	channel depth [m].
$\dot{\eta}$	aggradation rate [m/hr].
λ_p	bed material porosity.
Q_s	sediment discharge [m^3/hr].
Q	water discharge [m^3/hr].
S	downvalley slope.
D_{50}	median grain size [mm].
SLR	rate of sea level rise [mm/hr].
σ	subsidence rate [mm/hr].
f_{ch}	channel deposit fraction.
f_{ob}	overbank deposit fraction.

Acknowledgments. ADW thanks Matt Wolinsky, John Southard, Mariela Perignon, Peter Ashmore, and Bob Anderson for their insights. Reviews by Alex Densmore, Stephen Lancaster, and four anonymous reviewers helped us to improve the manuscript. This work was supported by the National Science Foundation (NSF) Research Experiences for Undergraduates program, the MIT UROP program through the Paul Gray UROP fund, and the Science and Technology Center program of the NSF via the National Center for Earth-Surface Dynamics under Agreement Number EAR-0120914.

References

- Alber, C., R. Ware, C. Rocken, and J. Braun (2000), Obtaining single path phase delays from GPS double differences, *Geophysical Research Letters*, 27(17), 2661–2664, doi: 10.1029/2000GL011525.
- Beard, D. C., and P. K. Weyl (1973), Influence of texture on porosity and permeability of unconsolidated sand, *AAPG Bulletin*, 57(2), 349–369.
- Bryant, M., P. Falk, and C. Paola (1995), Experimental study of avulsion frequency and rate of deposition, *Geology (Boulder)*, 23(4), 365–368, doi:10.1130/0091-7613(1995)023<0365:ESOFAFA>2.3.CO;2.
- Cazanacli, D., C. Paola, and G. Parker (2002), Experimental steep, braided flow: application to flooding risk on fans, *Journal of Hydraulic Engineering*, 128(3), 322–33, doi: 10.1061/(ASCE)0733-9429(2002)128:3(322).
- Church, M. (2006), Bed Material Transport and the Morphology of Alluvial River Channels, *Annual Review of Earth and Planetary Sciences*, 34(1), 325–354, doi: 10.1146/annurev.earth.33.092203.122721.
- Constantine, C. R., T. Dunne, and G. J. Hanson (2009), Examining the physical meaning of the bank erosion coefficient used in meander migration modeling, *Geomorphology*, 106(3-4), 242–252, doi:10.1016/j.geomorph.2008.11.002.
- Dickey, D. A., and W. A. Fuller (1979), Distribution of the Estimators for Autoregressive Time Series with a Unit Root, *Journal of the American Statistical Association*, 74(366a), 427–431, doi:10.1080/01621459.1979.10482531.
- Dickey, D. A., and W. A. Fuller (1981), Likelihood Ratio Statistics for Autoregressive Time Series with a Unit Root, *Econometrica*, 49(4), 1057, doi:10.2307/1912517.
- Dunne, T., J. A. Constantine, and M. B. Singer (2010), The Role of Sediment Transport and Sediment Supply in the Evolution of River Channel and Floodplain Complexity, *Transactions, Japanese Geomorphological Union*, 31(2), 155–170.
- Frazier, D. (1967), Recent deltaic deposits of the Mississippi River: their development and chronology, *Gulf Coast Association of Geological Societies Transactions*, 17, 287–315.
- Furbish, D. J. (1988), River-bend curvature and migration: How are they related?, *Geology*, 16(8), 752, doi:10.1130/0091-7613(1988)016<0752:RBCAMH>2.3.CO;2.
- Furbish, D. J. (1991), Spatial autoregressive structure in meander evolution, *Geological Society of America Bulletin*, 103(12), 1576–1589, doi:10.1130/0016-7606(1991)103<1576:GSAE>2.3.CO;2.
- Güneralp, I., and B. L. Rhoads (2009), Empirical analysis of the planform curvature-migration relation of meandering rivers, *Water Resources Research*, 45(9), 1–15, doi: 10.1029/2008WR007533.
- Güneralp, I., and B. L. Rhoads (2010), Spatial autoregressive structure of meander evolution revisited, *Geomorphology*, 120(3-4), 91–106, doi:10.1016/j.geomorph.2010.02.010.

- Güneralp, I., and B. L. Rhoads (2011), Influence of floodplain erosional heterogeneity on planform complexity of meandering rivers, *Geophysical Research Letters*, 38(14), 2–7, doi: 10.1029/2011GL048134.
- Hickin, E. J., and G. C. Nanson (1975), The character of channel migration on the Beatton River, north-east British Columbia, Canada, *Bulletin of the Geological Society of America*, 86(4), 487–494, doi:10.1130/0016-7606(1975)86<487:TCOCMO>2.0.CO;2.
- Hooke, J. M. (1980), Magnitude and distribution of rates of river bank erosion, *Earth Surface Processes*, 5(2), 143–157, doi: 10.1002/esp.3760050205.
- Hooke, R. L. (1975), Distribution of sediment transport and shear stress in a meander bend, *Journal of Geology*, 83(5), 543–565, doi:10.1086/628140.
- Howard, A. D. (2009), How to make a meandering river., *Proceedings of the National Academy of Sciences of the United States of America*, 106(41), 17,245–6, doi:10.1073/pnas.0910005106.
- Howard, A. D., and T. R. Knutson (1984), Sufficient conditions for river meandering: A simulation approach, *Water Resources Research*, 20(11), 1659–1667, doi:10.1029/WR020i011p01659.
- Jerolmack, D. J., and D. Mohrig (2007), Conditions for branching in depositional rivers, *Geology*, 35(5), 463–466, doi: 10.1130/G23308A.1.
- Kim, W., C. Paola, V. R. Voller, and J. B. Swenson (2006a), Experimental measurement of the relative importance of controls on shoreline migration, *Journal of Sedimentary Research*, 76(2), 270–283, doi:10.2110/jsr.2006.019.
- Kim, W., C. Paola, J. B. Swenson, and V. R. Voller (2006b), Shoreline response to autogenic processes of sediment storage and release in the fluvial system, *Journal of Geophysical Research*, 111, F04,013, doi:10.1029/2006JF000470.
- Kim, W., B. Sheets, and C. Paola (2010), Steering of experimental channels by lateral basin tilting, *Basin Research*, 22(3), 286–301, doi:10.1111/j.1365-2117.2009.00419.x.
- Leeder, M. R. (1978), A quantitative stratigraphic model for alluvium, with special reference to channel deposit density and interconnectedness, in *Canadian Society of Petroleum Geologists Memoir* 5, pp. 587–596.
- Martin, J., B. Sheets, C. Paola, and D. Hoyal (2009), Influence of steady base-level rise on channel mobility, shoreline migration, and scaling properties of a cohesive experimental delta, *Journal of Geophysical Research*, 114, F03,017, doi: 10.1029/2008JF001142.
- Martin, J. M. (2007), Quantitative sequence stratigraphy, Ph.D. thesis, University of Minnesota, Minneapolis, Minnesota, 55455, USA.
- McElroy, B., and D. Mohrig (2009), Nature of deformation of sandy bed forms, *Journal of Geophysical Research*, 114, F00A04, doi:10.1029/2008JF001220.
- Mohrig, D., P. L. Heller, C. Paola, and W. J. Lyons (2000), Interpreting avulsion process from ancient alluvial sequences; Guadalupe-Matarranya system (northern Spain) and Wasatch Formation (western Colorado), *Geological Society of America Bulletin*, 112(12), 1787–1803, doi:10.1130/0016-7606(2000)112<1787:IAPFAA>2.0.CO;2.
- Nanson, G. C., and E. J. Hickin (1983), Channel migration and incision on the Beatton River, *Journal of Hydraulic Engineering*, 109(3), 327–337, doi:10.1061/(ASCE)0733-9429(1983)109:3(327).
- Neill, C. (1971), River bed transport related to meander migration rates, *Journal of the Waterways, Harbors and Coastal Engineering Division*, 97(4), 783–786.
- Overeem, I., J. Syvitski, and E. Hutton (2005), Three-dimensional numerical modeling of deltas, in *River Deltas: Concepts, Models, and Examples*, edited by L. Giosan and J. P. Bhattacharya, SEPM Special Publication 83, pp. 13–30.
- Parker, G. (1979), Hydraulic geometry of active gravel rivers, *Journal of the Hydraulics Division*, 105(9), 1185–1201.
- Parker, G., Y. Shimizu, G. V. Wilkerson, E. C. Eke, J. D. Abad, J. W. Lauer, C. Paola, W. E. Dietrich, and V. R. Voller (2011), A new framework for modeling the migration of meandering rivers, *Earth Surface Processes and Landforms*, 36(1), 70–86, doi:10.1002/esp.2113.
- Pollen, N., and A. Simon (2005), Estimating the mechanical effects of riparian vegetation on stream bank stability using a fiber bundle model, *Water Resources Research*, 41(7), doi: 10.1029/2004WR003801.
- Popov, I. V. (1962a), A sediment balance of river reaches and its use for the characteristics of the channel process, *Soviet Hydrology (Trudy GGI)*, 1, 3–21.
- Popov, I. V. (1962b), Application of Morphological Analysis to the Evaluation of the General Channel Deformations of the River Ob', *Soviet Hydrology (Trudy GGI)*, 1, 267–324.
- Powell, E. J., W. Kim, and T. Muto (2012), Varying discharge controls on timescales of autogenic storage and release processes in fluvio-deltaic environments: Tank experiments, *Journal of Geophysical Research*, 117(F2), 1–14, doi: 10.1029/2011JF002097.
- Pyrce, R. S., and P. E. Ashmore (2003), Particle path length distributions in meandering gravel-bed streams: results from physical models, *Earth Surface Processes and Landforms*, 28(9), 951–966, doi:10.1002/esp.498.
- Reitz, M. D., and D. J. Jerolmack (2012), Experimental alluvial fan evolution: Channel dynamics, slope controls, and shoreline growth, *Journal of Geophysical Research*, 117(F2), 1–19, doi:10.1029/2011JF002261.
- Reitz, M. D., D. J. Jerolmack, and J. B. Swenson (2010), Flooding and flow path selection on alluvial fans and deltas, *Geophysical Research Letters*, 37(6), L06,401.
- Roberts, H. H. (1998), Delta switching: early responses to the Atchafalaya River diversion, *Journal of Coastal Research*, 14(3), 882–899.
- Sapozhnikov, V. B., and E. Foufoula-Georgiou (1997), Experimental evidence of dynamic scaling and indications of self-organized criticality in braided rivers, *Water Resources Research*, 33(8), 1983–1991.
- Sheets, B. A., C. Paola, and J. M. Kelberer (2007), Creation and preservation of channel-form sand bodies in an experimental alluvial system, in *Sedimentary processes, environments and basins: a tribute to Peter Friend*, edited by G. J. Nichols, E. Williams, and C. Paola, pp. 555–568, Blackwell, Oxford, UK.
- Simon, A., and A. J. C. Collison (2002), Quantifying the mechanical and hydrologic effects of riparian vegetation on streambank stability, *Earth Surface Processes and Landforms*, 27(5), 527–546, doi:10.1002/esp.325.
- Tal, M., and C. Paola (2007), Dynamic single-thread channels maintained by the interaction of flow and vegetation, *Geology*, 35(4), 347–350, doi:10.1130/G23260A.1.
- Tal, M., and C. Paola (2010), Effects of vegetation on channel morphodynamics: results and insights from laboratory experiments, *Earth Surface Processes and Landforms*, doi: 10.1002/esp.1908.
- Wickert, A. D. (2007), Measuring channel mobility through the analysis of area-based change in analog experiments, with insights into alluvial environments, S.b. thesis, Massachusetts Institute of Technology, Cambridge, MA, USA.
-
- A. D. Wickert, University of Colorado, Department of Geological Sciences and Institute of Arctic and Alpine Research, 1560 30th St., Boulder, CO 80303, USA. (wickert@colorado.edu)
- J. M. Martin, Integrated Reservoir Performance Prediction, ExxonMobil Upstream Research Company, P.O. Box 2189, (GW3-1034A), Houston, TX 77252-2189, USA. (john.m.martin@exxonmobil.com)
- M. Tal, Aix-Marseille Université, CEREGE UMR 7330, Europôle de l'Arbois, BP 80, 13545 Aix-en-Provence cedex 04, France. (tal@cerege.fr)
- W. Kim, The University of Texas at Austin, Department of Geological Sciences, 1 University Station C9000, Austin, TX 78712, USA. (delta@jsg.utexas.edu)
- B. Sheets, Barr Engineering Company, 4700 W. 77th St., Minneapolis, MN 55435, USA. (bsheets@barr.com)
- C. Paola, University of Minnesota, Department of Earth Sciences and St. Anthony Falls Laboratory, 2 Third Ave. SE, Minneapolis, MN 55455, USA. (cpaola@umn.edu)

Table 1. Experiment descriptions.

Experiment	Description	Reference
XES02-SS	Subsiding alluvial fan delta, stillstand phase	<i>Kim et al.</i> [2006a, b]
XES02-SF	—, slow base level fall phase	<i>Kim et al.</i> [2006a, b]
XES02-SR	—, slow base level rise phase	<i>Kim et al.</i> [2006a, b]
XES02-RF	—, rapid base level fall phase	<i>Kim et al.</i> [2006a, b]
XES02-RR	—, rapid base level rise phase	<i>Kim et al.</i> [2006a, b]
DB03-1	Alluvial fan delta with supercritical flow and constant sea level rise	<i>Sheets et al.</i> [2007]
DB03-2	Alluvial fan delta with subcritical flow and constant sea level rise	<i>Martin</i> [2007]
BV-1	Experimental braided stream	<i>Tal and Paola</i> [2007, 2010]
BV-2	—, forced with added vegetation	<i>Tal and Paola</i> [2007, 2010]

Table 2. Experimental channel system parameters and channel mobilities.

Experiment	f_w [–]	^a \bar{b} [m]	\bar{h} [m]	S [–]	Q_s [m ³ /hr]	Q [m ³ /hr]	^d D_{50} [mm]	ζ [m/hr]	SLR [mm/hr]	^e σ [mm/hr]	q_s [m/hr]	^f Ξ [–]
XES02-SS	0.1711	0.39	0.005	0.024	0.01822	1.5012	0.12	0.9927	0	1.85	9.34	0.11
XES02-SF	0.1746	0.44	0.009	0.036	0.01822	1.5012	0.12	1.0874	-2.26	1.85	4.60	0.24
XES02-SR	0.2327	0.5	0.008	0.022	0.01822	1.5012	0.12	1.1470	2.26	1.85	4.55	0.25
XES02-RF	0.2341	0.29	0.017	0.064	0.01822	1.5012	0.12	0.6297	-13.57	1.85	3.69	0.17
XES02-RR	0.4643	0.52	0.004	0.036	0.01822	1.5012	0.12	0.9395	13.57	1.85	8.76	0.11
DB03-1	0.0632	0.14	0.006	0.05	0.03600	1.44	0.12	2.7114	5	0	42.86	0.06
DB03-2	0.1801	0.47	0.003	0.009	0.00018	1.44	0.12	0.0283	0.023	0	0.13	0.22
BV-1	0.2763	^b 0.34	^b 0.012	0.015	0.00619	7.2	0.5	1.5554	0	0	1.52	1.02
BV-2	0.2954	^b 0.44	0.033	0.015	^c 0.00334	^c 7.2	0.5	0.0893	0	0	0.23	0.39

f_w : mean wetted fraction, \bar{b} : mean channel system width, \bar{h} mean depth, S : downvalley slope, Q_s : sediment discharge, Q : water discharge, D_{50} : median sediment diameter, ζ : rate of channel lateral motion, SLR: rate of sea-level rise, σ : subsidence rate, q_s : downstream sediment flux, Ξ : ratio of channel mobility to sediment flux (“efficiency” of cross-stream or morphologically-altering sediment transport).

^a Channel system mean width \bar{b} equals f_w times the width of the fluvial surface.

^b *Tal and Paola* [2007, 2010] see a larger wetted width in BV-1 than in BV-2 because they used a lower dye intensity threshold to define a channel.

^c This is the high-flow discharge, which the channel system experienced during our periods of observation.

^d Sediment in the delta experiments comprised both quartz and anthracite to simulate coarse and fine particles, respectively, due to the lower density of anthracite. These D_{50} values are given for quartz-density-equivalent grain sizes.

^e XES02 was run with a linear hinge-type subsidence [*Kim et al.*, 2006a, b]; the rate given here is the mean.

^f Ξ was calculated without accounting for channel mobility due to superelevation-driven avulsions (Equations 28 and 30) because we see no relationship between superelevation and ζ (Sections 6.2 and 6.3; Figure 8.C).

Table 3. Measured channel mobility parameters.

Experiment	Channel planform overlap				Fluvial surface reworking				Instantaneous mobility	
	a_M	M	p_M	R^2	a_R	R	p_R	R^2	ζ_f	[1/hr]
XES02-SS	0.7534	3.3261	0.0759	0.5287	0.8916	0.6482	0.1274	0.899	0.4355	
XES02-SF	0.8246	5.2873	0.1119	0.5653	0.9232	0.9214	0.1299	0.9484	0.5338	
XES02-SR	0.7608	4.5664	0.0504	0.5858	0.9006	1.3327	0.0712	0.8969	0.4315	
XES02-RF	0.7611	3.7436	0.0887	0.3809	0.8746	0.9209	0.0725	0.8964	0.8389	
XES02-RR	0.8823	6.2162	0.1008	0.5988	0.8955	2.7496	0.079	0.8609	0.5083	
DB03-1	—	—	—	0.3182	0.889	1.2103	0.0904	0.9446	1.224	
DB03-2	0.8664	0.1965	0.1601	0.5799	0.9704	0.0395	0.003	0.9634	0.01085	
BV-1	0.8493	1.7537	0.2069	0.8294	0.9218	0.6197	0.2067	0.9708	1.264	
BV-2	0.988	0.6474	0.6713	0.9211	0.9918	0.5293	0.8287	0.8267	0.05992	

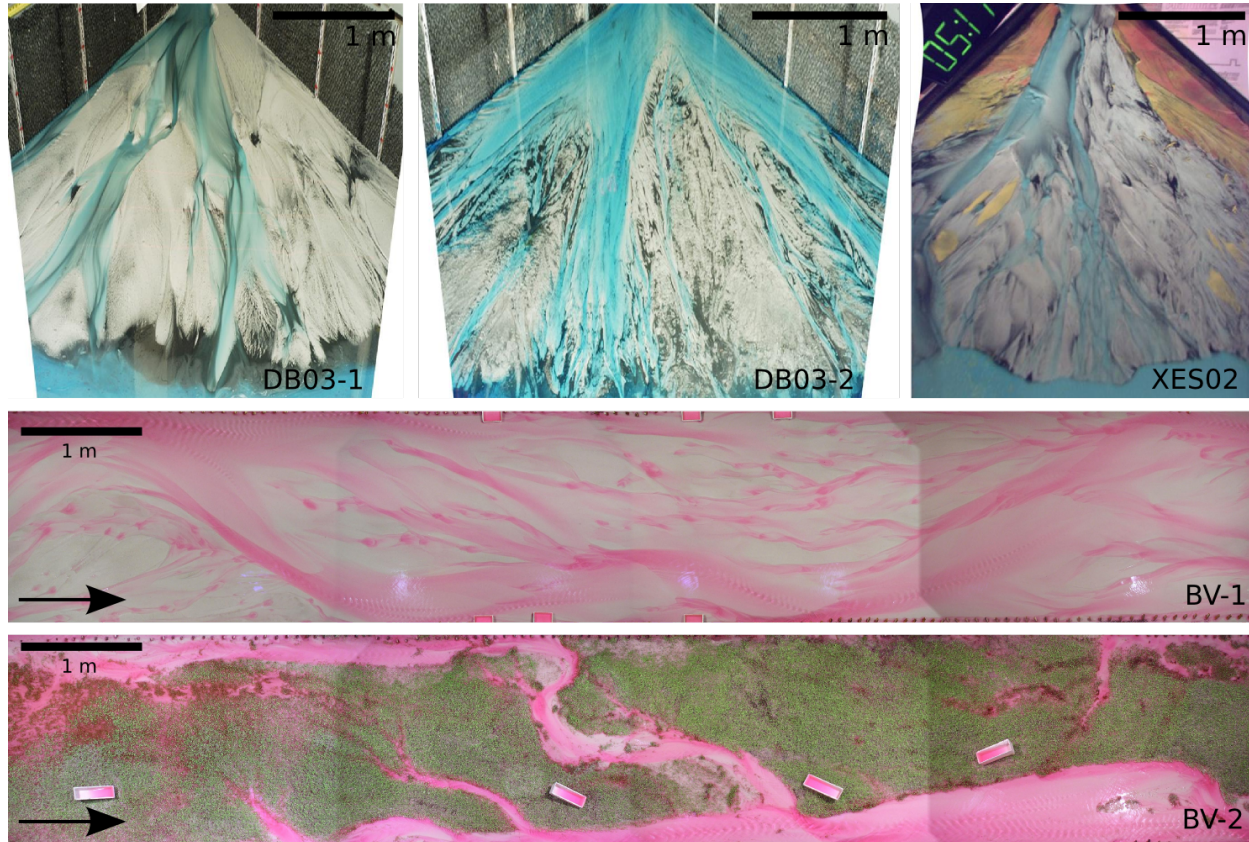


Figure 1. Laboratory experiments used for this study. DB03-1 and DB03-2 are twin experiments that prograded to a desired size and then aggraded with sea level rise to maintain constant surface area. Flow in DB03-1 was supercritical and flow in DB03-2 was subcritical. We analyze five periods of differing base level change for XES02 (Table 2). For BV, we study both the braided case (BV-1) and the fully vegetated case (BV-2); arrows show flow direction.

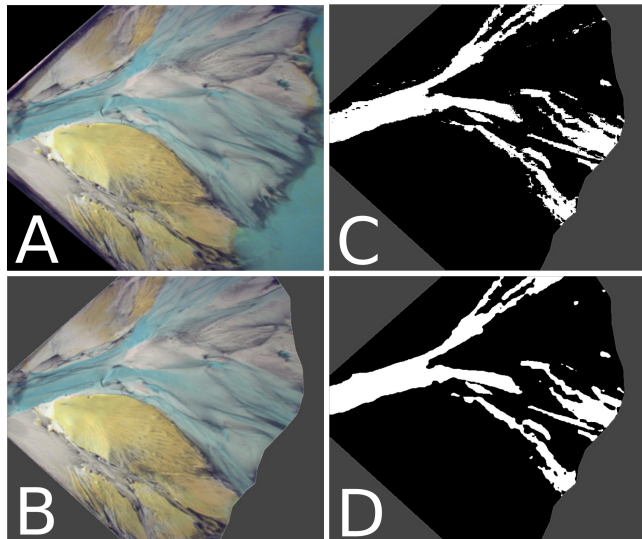


Figure 2. Steps to create the channel maps. First (A), the image is orthorectified and cropped. Second (B), the region outside the desired area is masked to the fluvial surface, F . Third (C), the images are separated by color into channel (“wet” area, white) and unoccupied fluvial surface (“dry” area, black). Fourth (D), the channel map is smoothed to remove small-scale noise. The example shown is XES02.

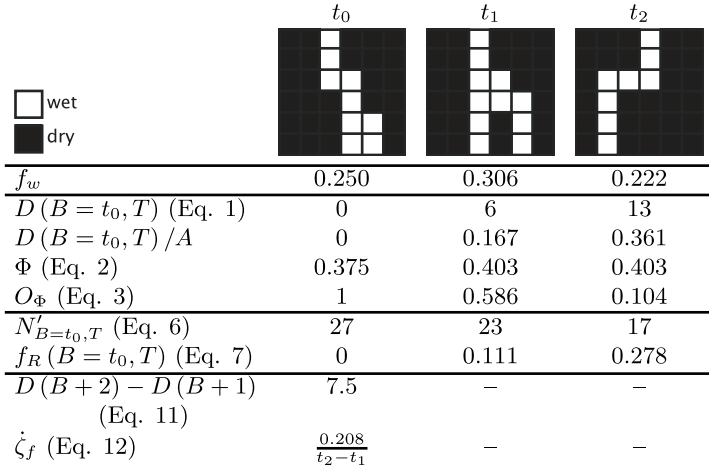


Figure 3. A schematic example of our analyses of river channel motion. The full fluvial surface is 36 cells large, with the squares in each of the channel maps representing very large pixels, and each channel map representing a different time step. The cartoon scenario presented is a river on a delta flowing towards the sea: in the second time step, a mouth bar is deposited, and in the third time step, the flow relocates. The calculations are separated into four sections. The first shows wetted (i.e. channel) fraction, f_w . The second shows the values used to calculate loss of planform overlap. These are D , the total number of pixels that change from dry to wet or wet to dry; D/A the number of changed pixels as a fraction of the total area of the fluvial surface; Φ , the fraction of overlap for a random scatter of wet and dry pixels; and O_Φ , the random-scatter-scaled amount of loss of planform overlap. The third set of variables include $N'_{B=t_0, T}$, the number of unreworked pixels, and f_R , the fraction of initially unoccupied pixels that have been reworked. The final two variables are used to compute instantaneous rates of channel motion: $D(B + 2) - D(B + 1)$, the double differenced amount of change between the channel maps at t_1 and t_2 , and $\dot{\zeta}_f$, the instantaneous rate of channel motion as a fraction of the fluvial surface area.

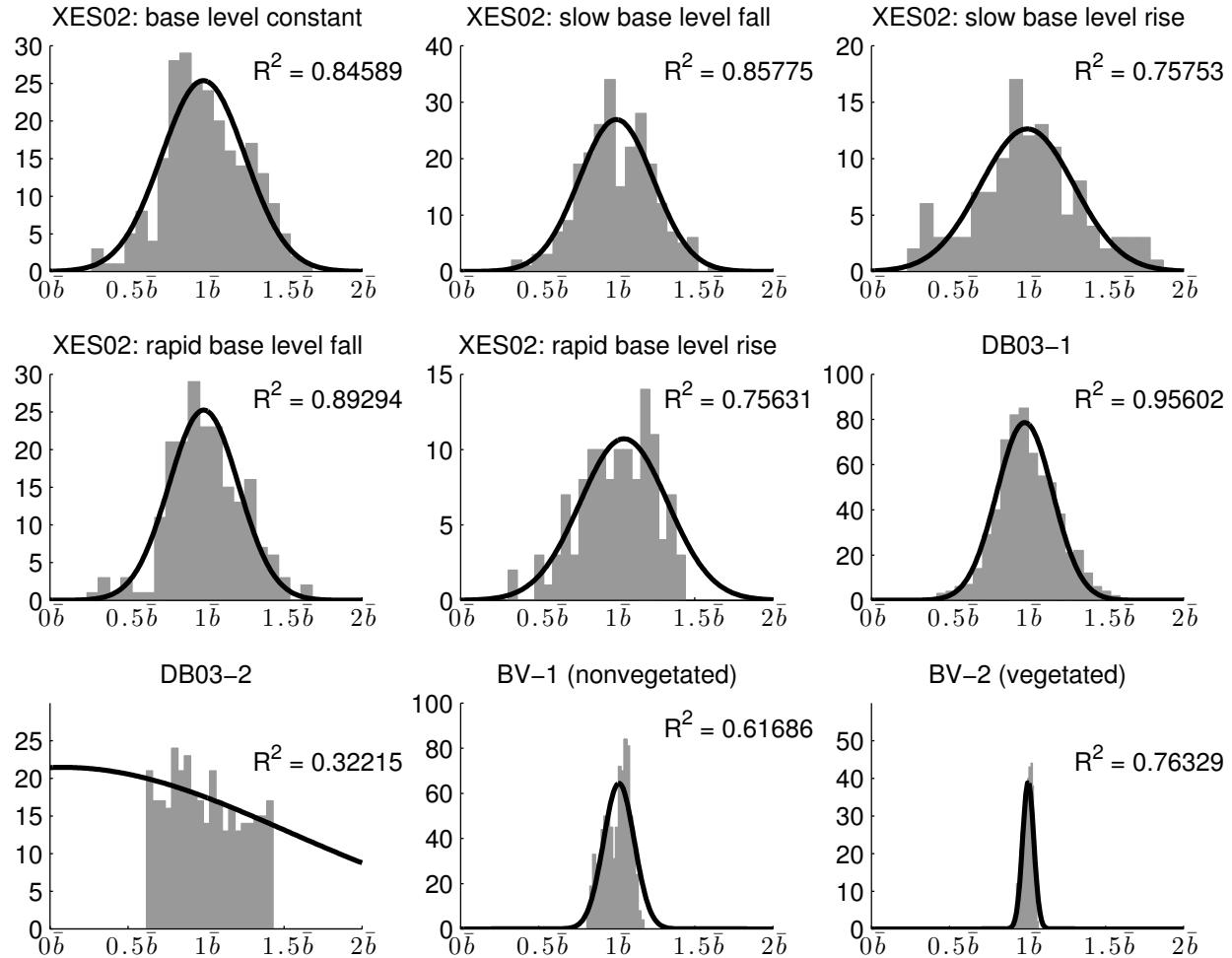


Figure 4. Channel widths are normally distributed. These histograms show variations in observed wetted area, which is directly related to channel width in all experiments but DB03-2, in which the dye intensity was variable. The *y*-axis gives the number of images in which a particular width bin appears, and the *x*-axis gives this width as a function of the mean width, \bar{b} . The R^2 values of the Gaussian function fits are listed on the plots.

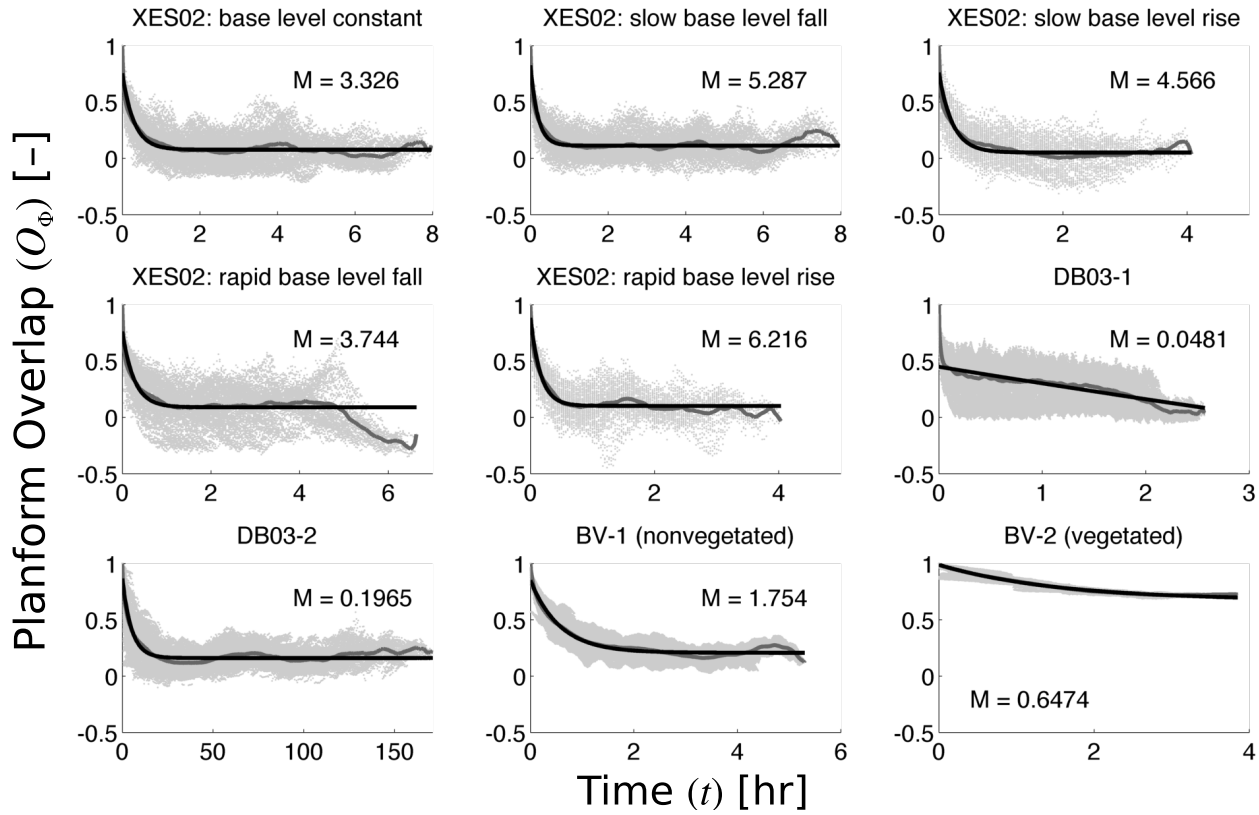


Figure 5. Loss of overlap with the original channel planform with time, scaled such that a value of 0 indicates the same amount of overlap as would be expected for random distributions of the same proportions of “wet” (channel) and “dry” (unoccupied fluvial surface) areas (Equations 2 and 3). Light gray point clouds are data from the experiments. Darker gray lines track the mean of these data points at each time step (i.e. they show the stacked data). Black lines show exponential decay fits given by Equation 4.1. (Parameters a_M , M , and p_M are given in Table 3.) The greater scatter observed in many of the deltas, and especially in DB03-1 (for which no good fit could be found), is due to patterns of lobe occupation and abandonment that cause periods of enhanced and weakened overlap with initial channel positions.

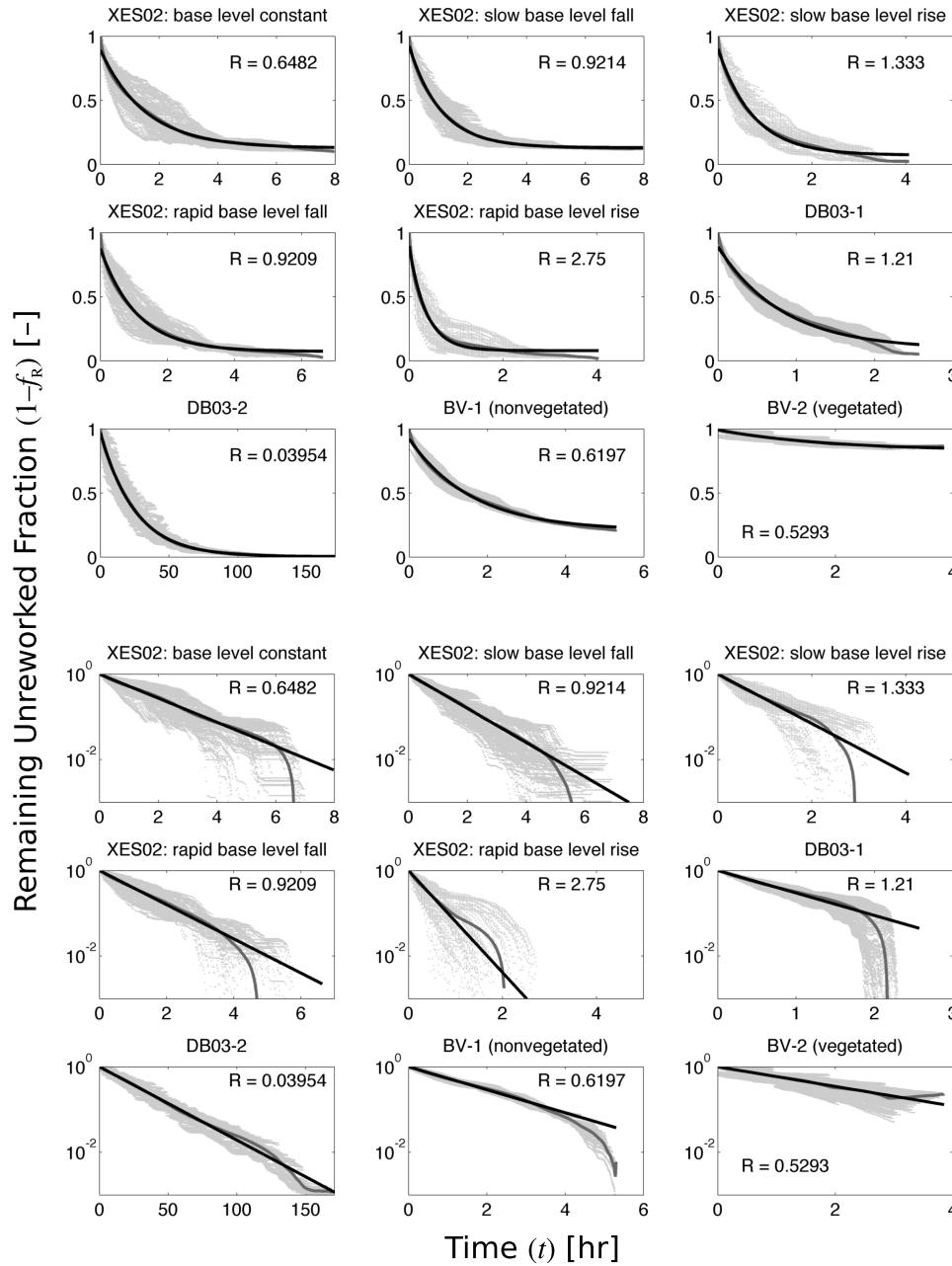


Figure 6. Fluvial surface reworking with time. Light gray point clouds are experimental data, and the darker gray lines track the mean of these data points at each time step (i.e. they show the stacked data). Black lines are exponential decay fits given by Equation 14, with parameters a_R , R , and p_R given in Table 3. The upper set of plots is on linear axes. The lower set has a logarithmic y-axis to better illustrate the exponential decay. Near the maximum times measured, many of the experiments show a downward departure from the exponential decay curve; this implies a longer-term process of visiting more rarely-occupied areas that may relate to the development and destruction of terraces in fluvial systems (see Section 7.2).

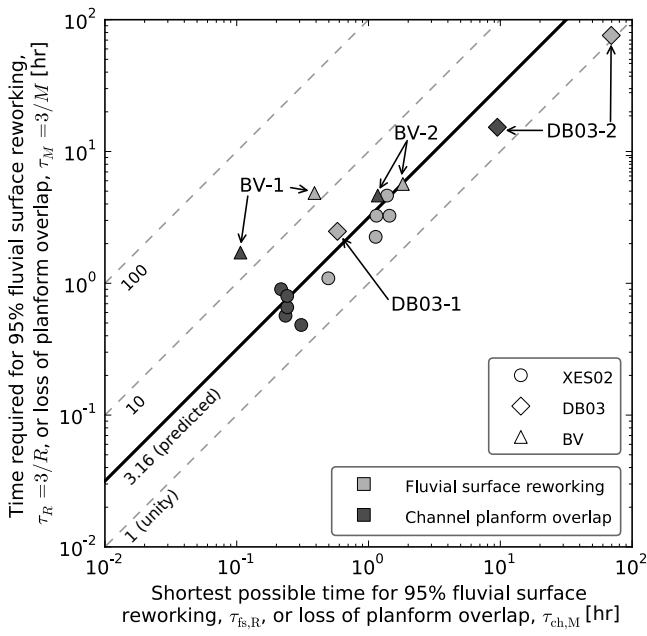


Figure 7. Comparisons between measured times and characteristic (most rapid possible: Equations 15 and 16) time scales for 95% fluvial surface reworking and loss of planform overlap. Labels by the lines are their slopes: Equation 26 predicts that the real channels will take 3.16 times as long to reach the 95% mark as the computed most rapid possible times. BV-1 retained a longer-term self-similarity that inhibited its ability to lose overlap with itself and rework its fluvial surface, while DB03-2 generated ripples that rapidly pushed its channels across its fan surface and increased its reworking efficiency (Section 5).

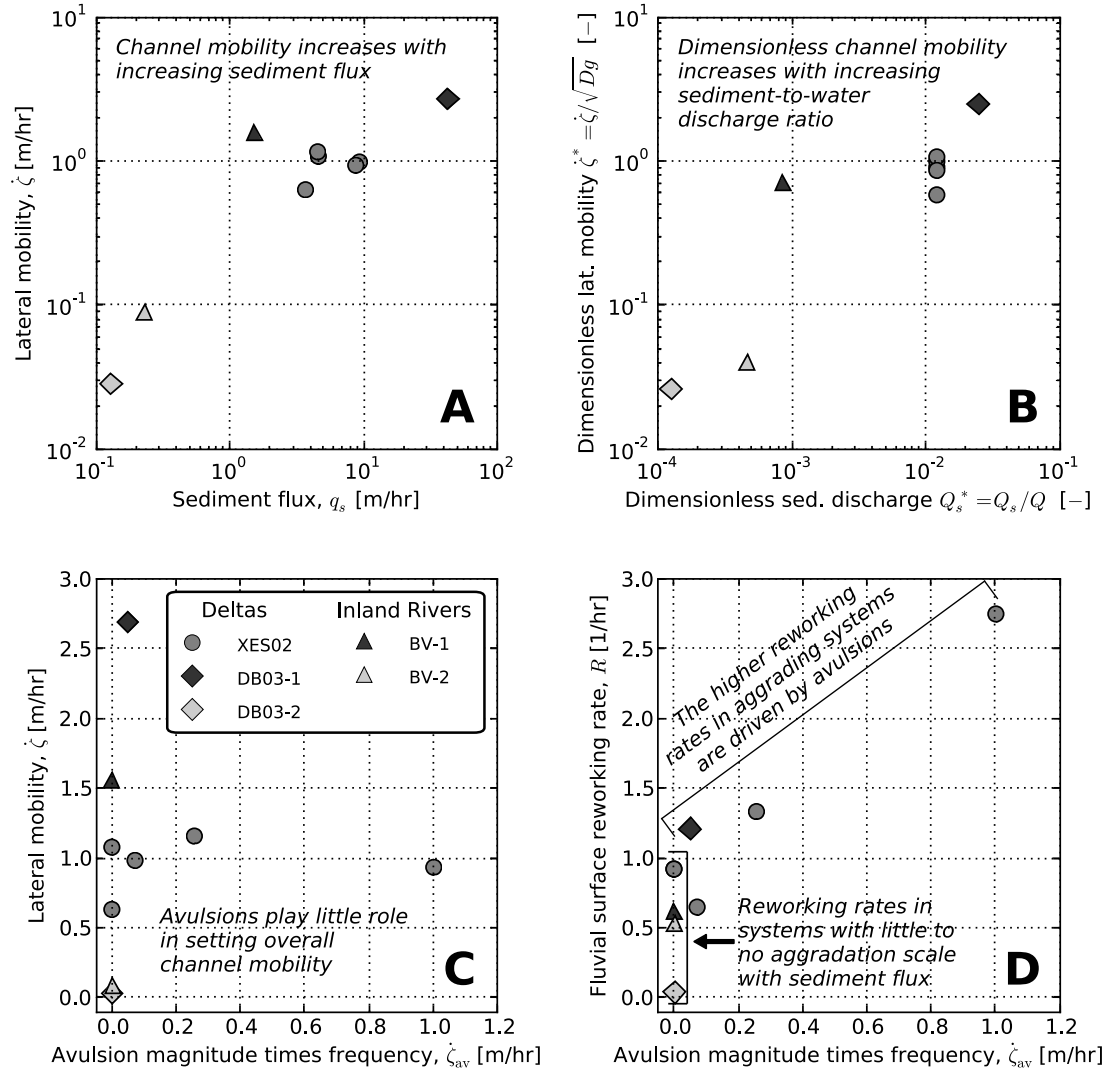


Figure 8. Sediment flux, aggradation, and channel mobility. The legend in **C** applies to all plots. **A** and **B** show a strong correlation between sediment transport and channel mobility; in Equation 29 we posit that for lateral migration dominated systems the dimensional form of this relationship should be linear with a slope of Ξ . The dimensionless relationship in **B** uses only terms that are inputs to fluvial system experiments. We see no relationship between our superelevation-based avulsion criterion and channel mobility (**C**), but we do see that the channel more rapidly visits and reworks its fluvial surface when the system is more avulsive (**D**). In **C** and **D**, XES02 (circles) is the most important data set because it experiences a range of aggradation rates due to variable base level change that is decoupled from its constant sediment input. In **D**, both points from the periods of base level fall in XES02 lie at approximately (0, 0.9).

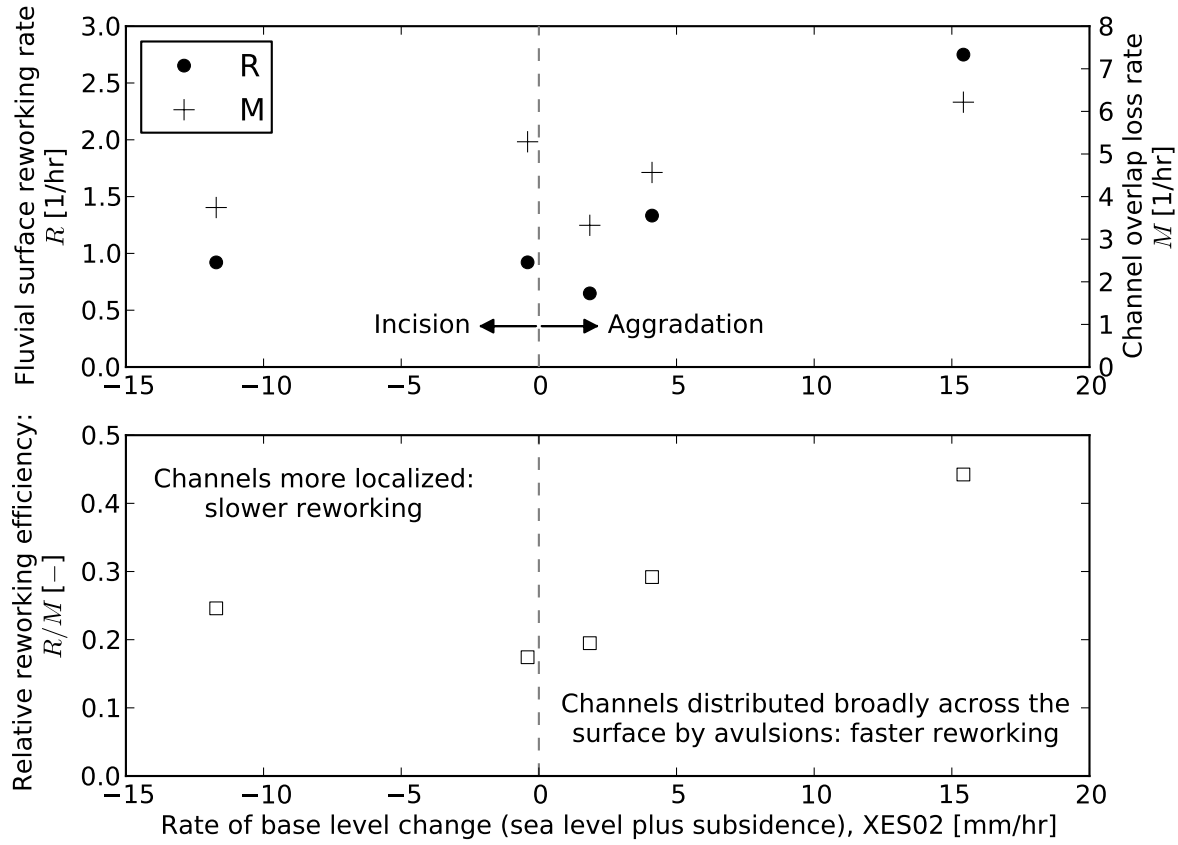


Figure 9. XES02 experienced cyclical base level changes. As the rate of base level rise increased, the channel more rapidly lost overlap with its old position (M) and reworked its fluvial surface (R). Base level fall and channel incision resulted in constant low reworking rates. Rates of loss of planform overlap during base level fall had approximately the same magnitude as those base level rise, showing that even without aggradationally-forced avulsions, lateral channel migration alone can produce comparable rates of loss of planform overlap. The bottom panel shows the relative speed of reworking when compared to loss of overlap: Rapid base level rise caused the channel to become more avulsive and more rapidly visit the whole fluvial surface. This ratio increases slightly with rapid base level fall, which may be an effect of decreased channel mobility in an incisional system.

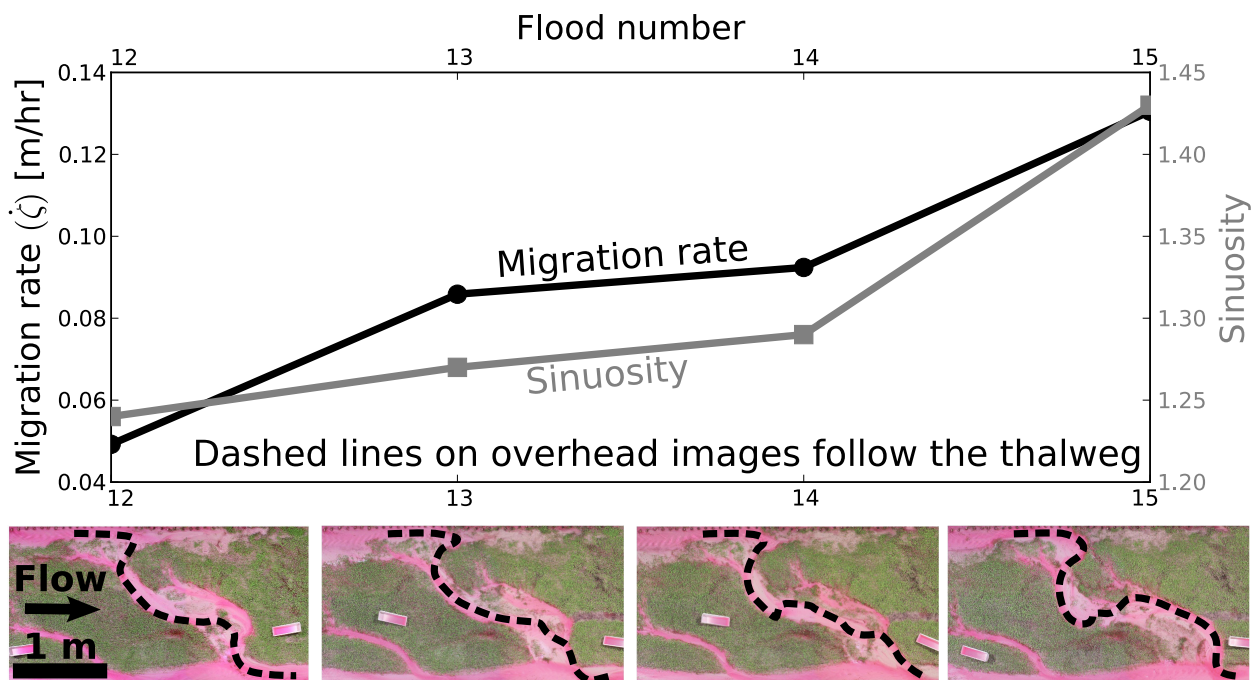


Figure 10. A reach in BV-2 became more sinuous from Flood 12 to Flood 15. To measure sinuosity, we traced a continuous thread of high dye intensity (i.e. deep flow) in images taken from halfway through each flood. The simultaneous increase in sinuosity and channel mobility illustrates a feedback by which a river bend produces gradients in shear stress and sediment transport capacity that lead to further erosion on the outer bank and deposition on the inner bank. Flow is from left to right.